Japanese Journal of Applied Physics

The Japan Society of Applied Physics

REGULAR PAPER

First-principles calculation of anomalous muonium in silicon: origin of the negative Fermi contact interaction constant

Japanese Journal of Applied Physics **58**, 081008 (2019) **REGULAR PAPER**
https://doi.org/10.7567/1347-4065/ab2f9a

First-principles calculation of anomalous muonium in silicon: origin of the negative Fermi contact interaction constant

Muhamad Nasruddin Manaf[1], Susumu Minami[1], Fumiyuki Ishii[2], and Mineo Saito[3*]

[1]*Graduate School of Natural Sciences and Technology, Kanazawa University, Kanazawa 920-1192, Japan*
[2]*Nanomaterials Research Institute, Kanazawa University, Kanazawa 920-1192, Japan*
[3]*Faculty of Mathematics and Physics, Kanazawa University, Kanazawa 920-1192, Japan*

[*]E-mail: m-saito@se.kanazawa-u.ac.jp

Received March 6, 2019; revised July 2, 2019; accepted July 5, 2019; published online July 29, 2019

We present the calculation of anomalous muonium in silicon which has been extensively studied but there still remains unresolved problems in the first-principles calculations. We perform calculations using spin-polarized density functional theory within the general gradient approximation or the local density approximation. We check the size effect of supercells and find that we need to use large sizes of supercells to obtain reliable results. Some quantitative disagreement between the experimental and theoretical values in previous studies may be due to the use of insufficient sizes of supercells. We clarify that the negative Fermi contact interaction constant (FCIC) is induced by the electron correlation effect. By using the Hubbard model, we find that the FCIC is zero when we neglect the correlation effect and the negative value of the FCIC is induced by the correlation effect.

1. Introduction

Defects in semiconductors have been attracting scientific interests for several decades.[1)] Defects cause significant effects on the electronic properties of semiconductors. Hydrogen is one of the most important impurities in materials and, in particular, in semiconductors.[2–7)] Hydrogen in semiconductors has favorable or unfavorable effects on the semiconductor devices. Hydrogen passivates shallow acceptors and donors, which has technologically unfavorable effects on semiconductor devices.[1)] On the other hand, recently it was suggested that hydrogen in semiconductors could act as a shallow impurity.[1,8–10)]

Muon spin resonance (μSR) is an effective tool to study hydrogen impurities in materials.[3,11)] The muon has the same electric charge as a proton. Although the mass is 1/9 of that of a proton, its behaviors in materials are expected to be similar to those of a proton. Thus, μSR is considered to be an effective tool to study protons or hydrogen.

In μSR, hyperfine parameters (HP), in particular, the Fermi contact interaction constants (FCIC) are observed. Analysis of these parameters provides useful information; for example, it gives information on the site of muonium, which is expected to be the stable site of hydrogen. To clearly determine the site, we need to perform first-principles calculations and compare the calculational and experimental results. Although an accumulation of theoretical studies has been conducted, a reliable method seems not to be established.

Muonium in silicon is one of the most extensively studied systems.[11–28)] Anomalous muonium was detected and was clearly identified as the muonium located at the bond center (BC) site, which is considered to be the most stable site.[22)] This anomalous muonium was reported by Patterson et al.[16)] and later the location was identified by Kiefl et al.[19)] who combined the level crossing resonance and μSR methods.

The HP at the BC site were calculated by several studies but, unfortunately, previous results largely deviate from the experimental data.[12,16,19,24,27)] The small sizes of supercells used in previous studies may be the reason for this discrepancy. Furthermore, the origin of the novel FCIC has not been clarified; the FCIC of the anomalous muonium is negative and the absolute value is extremely small.

In this paper, we attempt to perform reliable first-principles calculations of the FCIC of the muonium at the BC site in silicon. We perform spin-polarized density functional theory (DFT) calculations using supercell models to simulate the impurity in silicon. It is found that we need to check the convergence of the supercell size; the conventionally used supercell sizes are found to be insufficient to obtain reliable results. We clarify the origin of the small absolute value of the FCIC and discuss its negative sign.

2. Methods

2.1. Spin-polarized density functional calculations

First-principles calculations based on the spin-polarized DFT are carried out by using PHASE/0 code.[29–32)] In this calculation, we use a supercell approximation to study muonium in silicon crystals.[11,33)] The norm-conserving pseudopotential developed by Troullier and Martins is used for both atoms.[34)] We set the cut off energies 25 Rydberg and 100 Rydberg, respectively, for the wavefunctions and charge density. We use the local density approximation (LDA) and the generalized gradient approximation (GGA) for the exchange-correlation energy. The LDA calculation is based on the method developed by Perdew and Wang[35)] and we use the Perdew–Burke–Ernzerhof formalism for the GGA calculations.[36)]

The lattice parameter of the unit cell is set to be 5.431 Å which is deduced from the experimental data.[37–39)] We vary the size of the supercell, and then check the convergence of the FCIC. We adopt the Γk point sampling for supercell calculations. We optimize the atomic geometries and in the optimized geometry, the atomic forces are less than 10^{-3} Hartree/Bohr and the total energy is converged within 10^{-10} Hartree/cell. By using the k points of the $4 \times 4 \times 4$ mesh grid, we apply the tetrahedron method to the calculations of density of states (DOS) and projected density of states (PDOS).

2.2. Fermi contact interaction

The Hamiltonian for the hyperfine interaction is expressed as:

$$\mathcal{H} = \boldsymbol{S}^e \boldsymbol{A} \boldsymbol{S}^I, \tag{1}$$

where $\boldsymbol{S}^e, \boldsymbol{S}^I$ and $\boldsymbol{A}$ are electron spin, nuclear spin and hyperfine tensors, respectively. The hyperfine tensor consists of two parts, i.e., the isotropic part $\boldsymbol{A}_s$ and anisotropic part $\boldsymbol{A}_p$.

In this work, we focus on the isotropic part,which is expressed as:

$$\boldsymbol{A}_s = \frac{2\mu_0}{3}\hbar\gamma^e\gamma^I\rho_{\text{spin}}(0)\mathbf{1}, \tag{2}$$

where **1** is the 3×3 unit matrix. Equation (2) is expressed in the unit of MHz, where μ_0 ($4\pi \times 10^{-7}$ $\text{T}^2\text{m}^3\text{J}^{-1}$) is the permeability of vacuum, $\hbar$ ($1.054\,571\,68(18) \times 10^{-34}$ Js) is the reduced Plank constant, γ^e ($1.760\,859\,74(15) \times 10^{11}$ T^{-1} s^{-1}) is the electron gyromagnetic ratio and γ^I (133.81 MHz/T)[40] is the gyromagnetic ratio of nucleus. The $\rho_{\text{spin}}(0)$ is the spin density of electron at the nuclear position. The isotropic part of hyperfine tensor can be expressed as follows:

$$\boldsymbol{A}_s = A_s\begin{pmatrix}1 & 0 & 0\\ 0 & 1 & 0\\ 0 & 0 & 1\end{pmatrix}, \tag{3}$$

where A_s in Eq. (3) is the FCIC. For the free atom, the FCIC is expressed as follows:

$$A_s^{\text{free}} = \frac{2\mu_0}{3}\hbar\gamma^e\gamma^I|\phi_s(0)|^2, \tag{4}$$

where $|\phi_s(0)|^2$ is the electron spin density at the free muonium site, which originates from the s orbital. Since the electron density is equal to $1/\pi$, the value of A_s^{free} is equal to 4472 MHz.

We follow the method by Van de Walle and Blöch to evaluate the FCIC by using the pseudopotential calculations. To evaluate $\rho_{\text{spin}}(0)$, we use the following approximation[12,23]:

$$\rho_{\text{spin}}(0) = \tilde{\rho}_{\text{spin}}(\vec{R})\frac{|\phi_s(0)|^2}{|\tilde{\phi}_s(0)|^2}, \tag{5}$$

where $\tilde{\rho}_{\text{spin}}(0)$ is a pseudo-spin density at the muonium site and $|\tilde{\phi}_s(0)|^2$ is a pseudo-spin density of free muonium. Then the FCIC is given by[12,24]:

$$A_s = \frac{\tilde{\rho}_{\text{spin}}(0)}{|\tilde{\phi}_s(0)|^2}A_s^{\text{free}}. \tag{6}$$

To evaluate the reliability of the above approximation in the next section, we here introduce two quantities[12]:

$$\tilde{\eta} = \frac{\tilde{\rho}_{\text{spin}}(0)}{|\tilde{\phi}_s(0)|^2}, \tag{7}$$

where $\tilde{\eta}$ is the ratio of pseudo-spin density at the muonium site in silicon and pseudo-spin density of free muonium and

$$\eta = \frac{\rho_{\text{spin}}(0)}{|\phi_s(0)|^2}, \tag{8}$$

where η is the ratio of spin density at the muonium site in silicon from experimental data and spin density of free muonium.

3. Results and discussion

We first determine the stable position of muonium and confirm that the BC site is the most stable. Figure 1 shows the geometry of the present system. Table I tabulates the calculation results of the geometry of the muonium impurity at the BC site in silicon. We vary the supercell size and find that the $4 \times 4 \times 4$ supercell gives a well converged result.

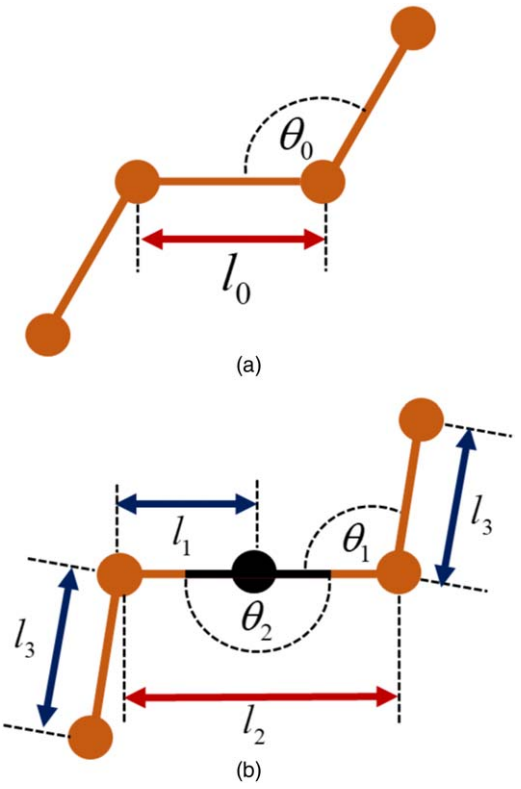

Fig. 1. (Color online) Geometries of pristine silicon (a) and muonium impurity at the BC site (b). $\theta_0 = 109.5^0$ and $l_0 = 2.35$ Å, respectively. The silicon and muonium atoms are denoted by the light brown sphere and dark sphere, respectively.

The bond lengths are slightly varied within 0.01 Å when we use the $5 \times 5 \times 5$ size supercell. We confirm that the Si–Mu–Si bond is linear and the distance between the nearest two silicon atoms is 3.220 Å. The distance between the nearest and the second nearest host atoms is close to the bond length of the perfect crystal, i.e., the difference is within 0.001 Å.

We next calculate the FCIC [Figs. 2(a) and 2(b)]. The constant reaches the convergence by using the $4 \times 4 \times 4$ size supercell. The supercell gives the value close to that from the value from the $5 \times 5 \times 5$ supercell calculation; the difference in the FCIC between these two supercells is small (5.47 MHz in the case of the GGA calculation). We find that the following function well fits to the above-mentioned FCIC

$$Y_{\text{FCIC}} = A + B\exp(-\alpha N), \tag{9}$$

where N is the the supercell parameter, which means that the supercell size is $N \times N \times N$. We find that the converged values for the GGA and LDA are -50.7 MHz and -15.0 MHz, respectively. The determined value of A, B, and α are tabulated in Table II.

The value calculated from the GGA calculation is found to be close to the experimental value.[19] The deviation of the above-mentioned converged value from the experimental one is 16.6 MHz (25%). This deviation is, in general, smaller than those in previous calculations (Table III). The deviations are 22.0 MHz−41.3 MHz (33%–61%). One of the reasons for the discrepancy between the experimental and calculational results in the past studies is expected to be due to the fact that small sizes of supercells were used.

We also evaluate the value of $\tilde{\eta}$ in Eq. (7) from calculational results and introduce the following fitting expression

Table I. Calculated geometry of the muonium impurity at the bond-centered (BC) site. The explanation of the geometrical parameters are given in Fig. 1.

Supercell size	Number of the silicon atoms	θ_1 (degree)		θ_2 (degree)		l_1 (Å)		l_2 (Å)		l_3 (Å)	
		LDA	GGA	LDA	GGA	LDA	GGA	LDA	GGA	LDA	GGA
$2 \times 2 \times 2$	64	99.9	99.9	180	180	1.619	1.619	3.238	3.237	2.312	2.313
$3 \times 3 \times 3$	216	99.7	99.8	180	180	1.624	1.619	3.247	3.239	2.320	2.321
$4 \times 4 \times 4$	512	99.8	99.8	180	180	1.614	1.614	3.228	3.227	2.322	2.322
$5 \times 5 \times 5$	1000	99.9	99.9	180	180	1.610	1.610	3.220	3.220	2.320	2.320

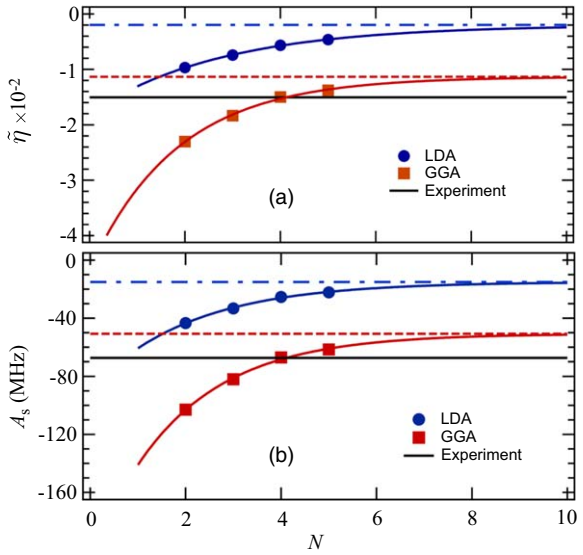

Fig. 2. (Color online) (a) Calculated $\tilde{\eta}$ given in Eq. (7). The black solid line represents η in Eq. (8) deduced from experimental data.[19] We present the fitting curves for the LDA and GGA calculational results. (b) Calculated FCIC. The experimental value is deduced from Ref. 19 and is represented by the black solid line. The horizontal axis represents N which means that the supercell size is $N \times N \times N$.

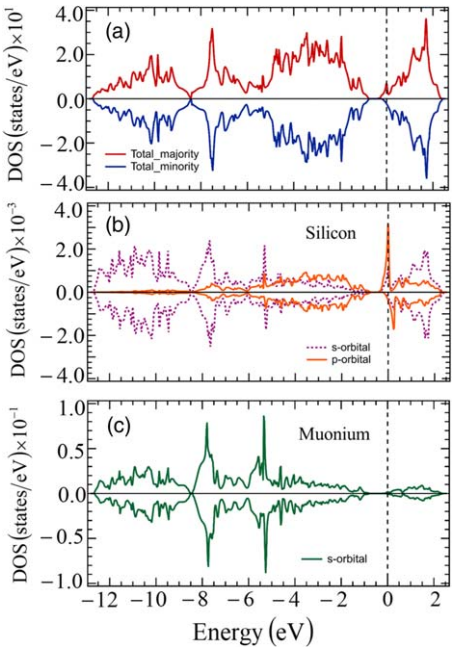

Fig. 3. (Color online) DOS (a) and PDOS of the nearest silicon atoms (b) and of the muonium (c). The vertical dashed lines indicate the Fermi level in the supercell calculations.

Table II. Fitting parameters in Eqs. (9) and (10).

Exchange Energy	A(MHz)	B(MHz)	α	A'	B'	α'
GGA	−50.7	−155.5	0.54	−0.011	−0.034	0.543
LDA	−15.0	−73.2	0.47	−0.002	−0.008	0.361

which is similar to Eq. (9):

$$Y_{\tilde{\eta}} = A' + B' \exp(-\alpha' N). \tag{10}$$

The determined parameters are tabulated in Table II. The converged value, A' (−0.011), is close to the value of η (−0.015) in Eq. (8) deduced from experimental data[19] (Fig. 2). This result suggests the validity of the approximation mentioned in the previous Sect. which was introduced in Ref. 12 and Ref. 23.

We here calculate the DOS, PDOS (Fig. 3) and spin density [Fig. 4(a)]. As the DOS [Fig. 3(a)] shows, the spin density mainly originates from the spin-polarized impurity level which is located below the conduction band bottom. By analyzing PDOS [Figs. 3(b) and 3(c)], we find that the impurity level mainly consists of the s and p orbitals of the nearest Si atoms and do not include the muonium s orbital component. As a result, the spin density is mainly distributed at the nearest two Si sites and the spin density is very small at the muonium site [Fig. 4(a)]. This is the reason why the

Table III. FCIC of muonium at the BC site. We show our calculational results for the 512, 1000 supercells and the converged value estimated by using Eq. (9).

References	Method	Exchange energy	Number of silicon atoms	FCIC (MHz)
Present	Pseudopotential	GGA	512	−67.1
Present	Pseudopotential	GGA	1000	−61.6
Present	Pseudopotential	GGA	Converged value	−50.7
Porter et al.[27]	All electron	GGA	16	−89.3
Porter et al.[27]	All electron	LDA	16	−27.1
Luchsinger et al.[24]	Pseudopotential	GGA	64	−81
Luchsinger et al.[24]	Pseudopotential	LDA	64	−26
Van de Walle and Blöchl[12]	Pseudopotential	LDA	32	−35
Experiment[19]				−67.3

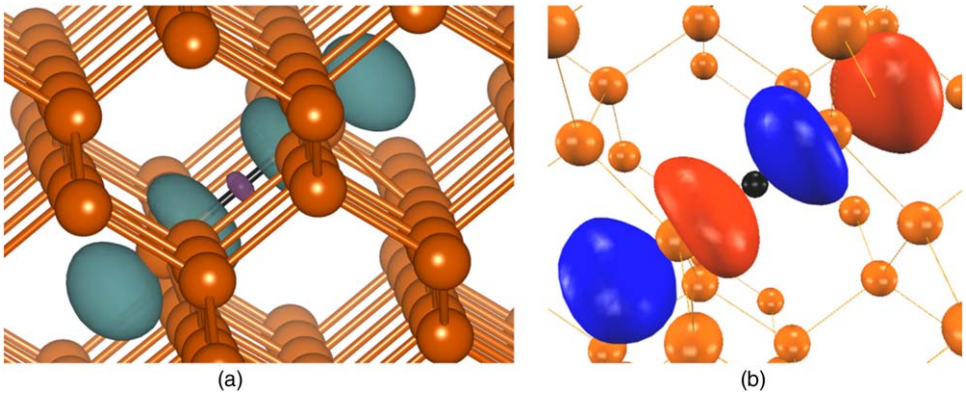

Fig. 4. (Color online) (a) Spin density where the absolute value of the isosurfaces is 1.50×10^{-3} Bohr^{-3}. The positive and negative spin densities are represented by green and purple colors, respectively. (b) Wavefunction of the impurity level. The red and blue colors represent positive and negative values, respectively.

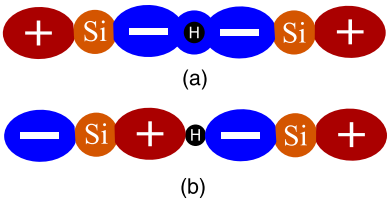

Fig. 5. (Color online) Schematic view of two muonium related wavefunctions. The red and the blue colors represent the positive and negative values, respectively.

absolute value of FCIC is very small in this system: The observed FCIC of the anomalous muonium is −67.3 MHz,[19] whose magnitude is much smaller than that of the free muonium (4463 MHz).[33]

Our calculation shows that the FCIC is negative, which is due to the fact that the spin density at the muon site is negative. We here discuss the origin of this negative spin density at the muon site. As was mentioned above, the impurity level does not contribute to the spin density at the muon site. Therefore, the spin density at the muon site is expected to originate from muon related states which are embedded in the valence band. Actually, the PDOS of the muon s orbital shows two strong peaks around −4 eV and −8 eV [Fig. 3(c)]. The minority spin DOS at these peaks are found to be larger than those of the majority spin DOS. This difference causes the negative spin density at the muonium site.

We here introduce a simplified model to explain the above results concerning the negative spin density. In Fig. 5, we consider two wavefunctions. In the wavefunction in Fig. 5(a), the nearest Si orbitals and muonium s orbital have the same phases (bonding) and in the other wavefunction in Fig. 5(b), the two Si p orbitals have anti-phase, therefore there is the node at the muonium site. Since the former wavefunction has a relatively low energy, it is embedded in the valence band. Since the wavefunction has an amplitude at the muonium site, it contributes to the small but finite value of the FCIC. On the other hand, since the latter wavefunction has a relatively higher energy, it is included in the impurity level [Fig. 4(b)] and does not contribute to the FCIC.

To clearly understand the novel FCIC, we here introduce the linear tri-hydrogen molecule, which is considered to be a simplified model of the present system (Fig. 6). First, we

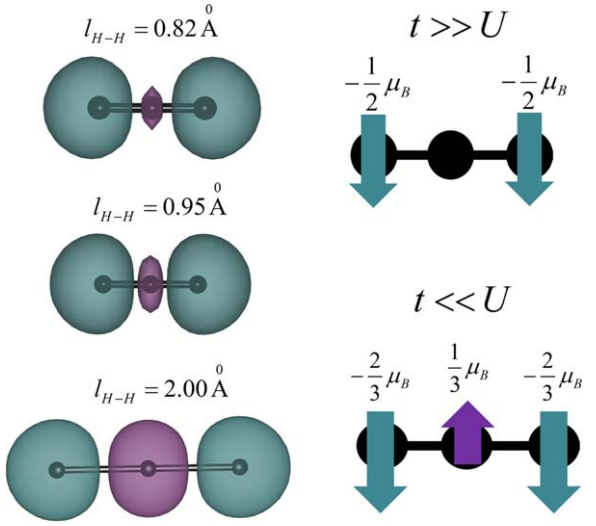

Fig. 6. (Color online) Spin densities of the linear tri-hydrogen molecule (the green and the purple colors represent positive and negative value of isosurfaces, respectively) for the cases of $l_{H-H} = 0.82$ Å (the isosurface value is 9.11×10^{-2} spin/Bohr^{-3}), $l_{H-H} = 0.95$ Å (the isosurface value is 4.11×10^{-2} spin/Bohr^{-3}), and $l_{H-H} = 2.0$ Å (the isosurface value is 4.11×10^{-2} spin/Bohr^{-3}). We also show the magnetic moment at each site calculated based on the Hubbard model. Two limiting cases ($t \gg U$ and $t \ll U$) are considered.

consider a tight binding model including a hopping parameter t between the nearest atomic sites. Two electrons with majority and minority spins occupy the lowest energy level, $\phi_1 = \frac{1}{2}(\chi_1 + \sqrt{2}\chi_2 + \chi_3)$, where χ_1 and χ_3 are the atomic orbitals at the two side sites and χ_2 is the orbital at the middle site. This wavefunction corresponds to that in Fig. 5(a). A single majority spin electron occupies the second lowest level, $\phi_2 = \frac{1}{\sqrt{2}}(\chi_1 - \chi_3)$, which corresponds to that in Fig. 5(b). Therefore, the tight binding approximation leads to the result that the spin density at the middle site is zero and the spin density appears at the both side sites (each side site has the magnetic moment of 0.5 μ_B and the middle site has no magnetic moment) (see Fig. 6). We perform a GGA calculation on the linear tri-hydrogen molecule by taking the equilibrium bond length ($l_{H-H} = 0.95$ Å) and obtain results which are similar to those based on the tight binding model. As Fig. 7 shows, low energy levels occupied by majority and minority spin electrons have wavefunctions similar to ϕ_1 and a high energy level occupied by a single majority spin

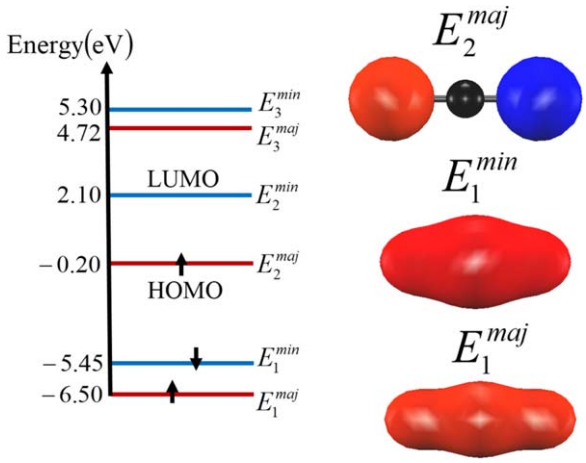

Fig. 7. (Color online) Schematic diagram of energies of the linear tri-hydrogen molecule on the left hand side and wavefunctions on the right hand side where the red and blue colors represent positive and negative amplitudes, respectively.

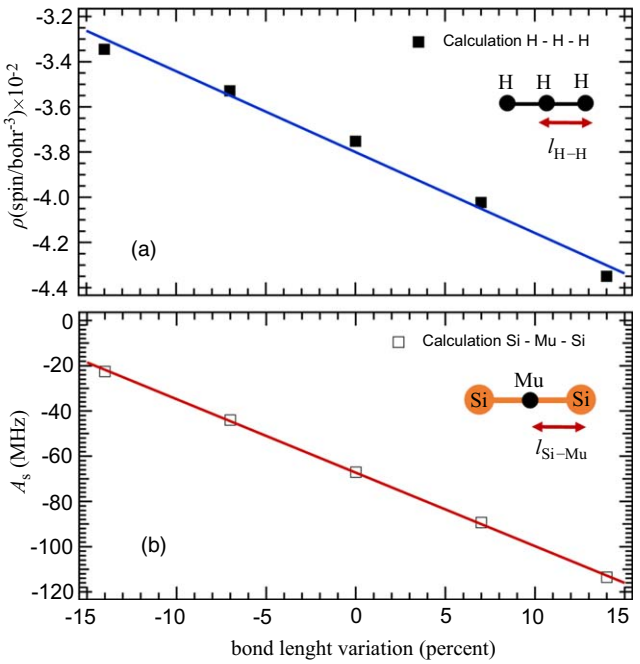

Fig. 8. (Color online) (a) Spin density of the linear tri-hydrogen molecule. We carry out calculations by changing the bond length from the equilibrium bond length ($l_{H-H} = 0.95$ Å). (b) FCIC of anomalous muonium in silicon. The calculations are performed by changing the bond length from the equilibrium one ($l_{Si-Mu} = 1.61$ Å).

electron has a wavefunction similar to ϕ_2. However, there is a slight difference between the ϕ_1 type wavefunctions occupied by majority spin and minority spin electrons. As a result, the middle site has a small amount of the spin density which is negative. This small value of the spin density cannot be explained based on the tight binding model which leads to the zero value of the spin density, so we expect that the nonzero value originates from the electron correlation effect.

We hence introduce the Hubbard model including the on-site Coulomb repulsion U as well as t.[41] We numerically solve the Hubbard model in the case of $\frac{t}{U} \to 0$, and find that the magnetic moments at the middle site and the side sites have opposite signs. The magnetic moment at the middle site and the edge sites are $\frac{1}{3}\mu_B$ and $-\frac{2}{3}\mu_B$, respectively (see Fig. 6), which means that the spin density at the middle site is negative. We perform GGA calculations by taking a large bond length ($l_{H-H} = 2.0$ Å), which corresponds to a small $\frac{t}{U}$ case in the Hubbard model (see Fig. 6). The calculated spin density distribution is similar to that in the Hubbard model in the limit, $\frac{t}{U} \to 0$.

As $\frac{t}{U}$ becomes large, the magnitude of the spin density at the middle site is expected to decrease and get close to zero as is expected based on the tight binding model. This tendency of the spin density expected based on the Hubbard model is reproduced by our GGA calculation. We perform calculations for the bond lengths of 0.82 Å, 0.95 Å and 2.00 Å and find that the magnitude of the spin density at the middle site becomes small as the bond length decreases (Fig. 6). This tendency of the spin density is also demonstrated in Fig. 8(a). We plot the spin densities by varying the bond lengths around the equilibrium length (0.95 Å). The magnitude of the negative spin density linearly decreases as the bond length becomes small. Since a shorter bond corresponds to a larger t, the above-mentioned results calculated based on the GGA are consistent with those based on the Hubbard model. We conclude that the negative spin density at the middle site is due to the electron correlation effect since it arises when U is not zero.

The spin density distribution in muonium in silicon is expected to be similar to that of the linear tri-hydrogen molecule where the two nearest Si atoms in the present system are substituted by hydrogen atoms. To confirm this expectation, we perform GGA calculations for various Si–Mu bond lengths. We displace the nearest two Si atoms from the equilibrium positions. As a result, we find that the magnitude of the negative FCIC becomes large as the Si–Mu bond length increases [Fig. 8(b)]. This bond length dependence of the FCIC is similar to that in the case of the spin density at the middle site in linear tri-hydrogen molecules. We expect that small magnitude of the FCIC corresponds to the case of a large $\frac{t}{U}$ in the Hubbard model for the linear tri-hydrogen molecule. It is noted, however, that the present Si–Mu bonds are resonant and thus the length (1.619 Å) is much longer than the conventional Si–Mu bond length; for example, the silane (SiH_4) forms the bonds whose lengths are 1.481 Å[42]. This rather long bond length is expected to enhance the magnitude of the FCIC compared with the cases of shorter bond lengths. Finally, by considering the analogy between the linear tri-hydrogen molecule and the present system, we attribute the negative FCIC to the electron correlation effect.

4. Conclusion

We have performed first-principles calculations of anomalous muonium in silicon and by using the GGA, we succeeded in reproducing the experimental FCIC. The constant is negative and its magnitude is extremely small. We found that a large supercell is necessary to obtain the converged result. We clarified the origin of the very small magnitude of the FCIC and discuss the origin of the negative value. By considering the analogy between the linear tri-hydrogen molecule and the present system, we concluded that the negative value is induced by the electron correlation effect.

Acknowledgments

This work was partly supported by Grants-in-Aid for Scientific Research (No. 17K05118) from the Japan Society

for the Promotion of Science (JSPS). The computations in this research were performed using the supercomputers at the Institute for Solid State Physics (ISSP) at the University of Tokyo. The spin densities in Fig. 4(a) and 6 were drawn using VESTA.[43,44] The authors wish to thank Dr. Sholihun and Mr. Naoya Yamaguchi due to a valuable discussion. M.N.M. gratefully acknowledges a scholarship from the Ministry of Education, Culture, Sports, Science and Technology of Japan.

ORCID iDs

Muhamad Nasruddin Manaf https://orcid.org/0000-0003-0923-421X
Susumu Minami https://orcid.org/0000-0002-2852-3503
Fumiyuki Ishii https://orcid.org/0000-0003-2721-7675

1) H. J. Queisser and E. E. Haller, Science **281**, 945 (1998).
2) J. Pankove and N. M. Johnson (ed.) *Hydrogen in Semiconductors* (Academic, New York, 1991).
3) R. L. Lichti, in *Protons and Muons in Materials Science*, ed. E. A. Davies and S. F. J. Cox (Taylor and Francis, London, 1996).
4) C. G. Van de Walle and J. Neugebauer, Nature **423**, 626 (2003).
5) T. Sasaki and H. Katayama-Yoshida, J. Phys. Soc. Jpn. **58**, 1685 (1989).
6) J. I. Pankove, D. E. Carlson, J. E. Berkeyheiser, and R. O. Wance, Phys. Rev. Lett. **51**, 2224 (1983).
7) N. M. Johnson, C. Herring, and D. J. Chadi, Phys. Rev. Lett. **56**, 769 (1986).
8) K. Shimomura, R. Kadono, K. Ohishi, M. Mizuta, M. Saito, K. H. Chow, B. Hitti, and R. L. Lichti, Phys. Rev. Lett. **92**, 135505 (2004).
9) K. Shimomura et al., Physica B **376–377**, 444 (2006).
10) B. Monemar, P. P. Paskov, J. P. Bergman, M. Iwaya, S. Kamiyama, H. Amano, and I. Akasaki, Physica B **376–377**, 460 (2006).
11) B. D. Patterson, Rev. Mod. Phys. **60**, 69 (1988).
12) C. G. Van de Walle and P. E. Blöchl, Phys. Rev. B **47**, 4244 (1993).
13) Y. V. Gorelkinskii and N. N. Nevinnyi, Pi'sma Zh. Tekh. Fiz. **13**, 105 (1987).
14) Y. V. Gorelkinskii and N. N. Nevinnyi, Sov. Tech. Phys. Lett. **13**, 45 (1987).
15) K. M. Crowe, R. F. Johnson, J. H. Brewer, F. N. Gygax, D. G. Fleming, and A. Schenck, Bull. Am. Phys. Soc. **17**, 594 (1972).
16) B. D. Patterson et al., Phys. Rev. Lett. **40**, 1347 (1978).
17) J. S. Wang and C. Kittel, Phys. Rev. B **7**, 713 (1973).
18) J. H. Brewer et al., Phys. Rev. Lett. **31**, 143 (1973).
19) R. F. Kiefl, M. Celio, T. L. Estle, S. R. Kreitzman, G. M. Luke, T. M. Riseman, and E. J. Ansaldo, Phys. Rev. Lett. **60**, 224 (1988).
20) S. F. J. Cox and M. C. R. Symon, Chem. Phys. Lett. **126**, 516 (1986).
21) D. M. Maric, S. Vogel, P. F. Meier, and S. K. Estreicher, Hyperfine Interact **64**, 573 (1990).
22) P. R. Briddon and R. Jones, Hyperfine Interact **64**, 593 (1990).
23) C. G. Van de Walle, Phys. Rev. Lett. **64**, 669 (1990).
24) R. H. Luchsinger, Y. Zhou, and P. Meier, Phys. Rev. B **55**, 6927 (1997).
25) T. Miyake, T. Ogitsu, and S. Tsuneyuki, Phys. Rev. Lett. **81**, 1873 (1998).
26) T. Miyake, T. Ogitsu, and S. Tsuneyuki, Phys. Rev. B **60**, 14197 (1999).
27) A. R. Porter, M. D. Towler, and R. J. Needs, Phys. Rev. B **60**, 13534 (1999).
28) L. Liborio, S. Sturniolo, and D. Jochym, J. Chem. Phys. **148**, 134114 (2018).
29) P. Hohenberg and W. Kohn, Phys. Rev. **136**, B864 (1964).
30) W. Kohn and L. J. Sham, Phys. Rev. **140**, A1133 (1965).
31) T. Ohno, T. Yamamoto, T. Kokubo, A. Azami, Y. Sakaguchi, T. Uda, T. Yamasaki, D. Fukata, and J. Koga, SC '07: Proc. 2007 ACM/IEEE Conf. on Supercopm, 2007, 57.
32) M. C. Payne, M. P. Teter, D. C. Allan, T. A. Arias, and J. D. Joannopoulos, Rev. Mod. Phys. **64**, 1045 (1992).
33) J. S. Möller, D. Ceresoli, T. Lancaster, N. Marzari, and S. J. Blundell, Phys. Rev. B **87**, 121108(R) (2013).
34) N. Troullier and J. L. Martins, Phys. Rev. B **43**, 1993 (1991).
35) J. P. Perdew and Y. Wang, Phys. Rev. B **45**, 13244 (1992).
36) J. P. Perdew, K. Burke, and M. Ernzerhof, Phys. Rev. Lett. **77**, 3865 (1996).
37) https://crystdb.nims.go.jp/.
38) Y. Miyamoto and M. Hirata, J. Phys. Soc. Jpn. **44**, 181 (1978).
39) Y. Okada and Y. Tokumaru, J. Appl. Phys. **56**, 314 (1984).
40) D. R. Lide (ed.) *CRC Handbook of Chemistry and Physics* (Taylor and Francis, Boca Raton, FL, 2007) 87th ed.
41) J. Hubbard, Proc. R. Soc. Lond. **276**, 1365 (1963).
42) A. F. Holleman and E. Wiberg, *Inorganic Chemistry* (Academic, London, 2001).
43) http://jp-minerals.org/vesta.
44) K. Momma and F. Izumi, J. Appl. Crystallogr. **44**, 1272 (2011).